Open-source software for ultrasound-based guidance in spinal fusion surgery

Houssem-Eddine Gueziri[a,*], Charles X. B. Yan[b], D. Louis Collins[a]

[a] *McConnell Brain Imaging Center, Montreal Neurological Institute and Hospital, McGill University, Montreal (QC), Canada.*

[b] *Joint Department of Medical Imaging, University of Toronto, Toronto (ON), Canada.*

Abstract

Spinal instrumentation and surgical manipulations may cause loss of navigation accuracy requiring an efficient re-alignment of the patient anatomy with preoperative images during surgery. While intra-operative ultrasound (iUS) guidance has shown clear potential to reduce surgery time, compared to clinical CT guidance, rapid registration aiming to correct for patient misalignment has not been addressed. In this paper, we present an open-source platform for pedicle screw navigation using iUS imaging. The alignment method is based on rigid registration of CT to iUS vertebral images and has been designed for fast and fully automatic patient re-alignment in the operating room (OR). Two steps are involved: first, we use the iUS probe's trajectory to achieve an initial coarse registration; then, the registration transform is refined by simultaneously optimizing gradient orientation alignment and mean of iUS intensities passing through the CT-defined posterior surface of the vertebra. We evaluated our approach on a lumbosacral section of a porcine cadaver with 7 vertebral levels. We achieved a median target registration error (TRE) of 1.47 mm (100 % success rate, defined by TRE < 2 mm) when applying the probe's trajectory initial alignment. The approach showed a high robustness to partial visibility of the vertebra with success rates of 89.86 % and 88.57 % when missing either the left or right parts of the vertebra; and robustness to initial misalignments with a success rate of 83.14 % for random starts within $\pm 20^\circ$ rotation and ± 20 mm translation. Our GPU implementation achieves an efficient registration time under 8 s, which makes the approach suitable for clinical application.

Keywords: Registration, Open-source navigation platform, Spinal fusion surgery, Ultrasound guidance, Computed Tomography, GPU.

Introduction

Spinal fusion procedures are employed for many surgical treatments of pathological spine instabilities. The surgery aims at correcting spinal deformity, such as severe scoliosis, or limiting the inter-vertebral movements in the case of spinal degenerative changes, disk disorder or spinal stenosis (Deyo et al., 2004). The instrumentation involves implanting screws into the pedicles in order to stabilize the spine with metal rods and bone grafts. While the placement of pedicle screws is associated with risks of neurological and/or vascular injuries, intra-operative 2D fluoroscopy or 3D computed tomography (CT) guidance have shown to decrease breach and screw malpositioning rates (Smith et al., 2014; Austin et al., 2002; Gebhard et al., 2004). However, the imaging protocol exposes the patient and the operating room (OR) personnel to risks of harmful radiation, precluding frequent acquisitions. In addition, the acquisition time is estimated to be 15-20 minutes, which significantly interrupts the surgical workflow.

Image-guided surgery (IGS) is based on the

*Corresponding Author: Houssem-Eddine Gueziri, Montreal Neurological Institute and Hospital, 3801 University Street, WB 221, Montreal, QC H3A 2B4, Canada; Email, houssem.gueziri@mcgill.ca

registration established between pre- or intra-operative images and the current position of the patient, allowing for tracking surgical tools with respect to the anatomy. A common issue in IGS is the loss of navigation accuracy as the duration of the surgery increases (Quiñones-Hinojosa et al., 2006; Stieglitz et al., 2013). Drilling and taping instrumentation, as well as repetitive contact with bone tissues may cause non-intentional displacement of the tracked reference attached to the vertebra. As a result, the registration established at the beginning of surgery is rendered invalid.

Alternative approaches have been investigated to reduce radiation exposure. Stereovision has been employed in open spine surgery, where the reconstruction of exposed posterior surface of vertebrae was registered with pre-operative CT (Ji et al., 2015). Only a few cases of intra-operative magnetic resonance (MR) use in spine surgery have been reported (Woodard et al., 2001; Takahashi et al., 2008, 2009; Tatsui et al., 2017). While MR imaging provides a good soft tissue visualization, it is associated with high costs and non-magnetic surgical instruments constraints, limiting its use in the OR. Intra-operative ultrasound (iUS) guidance has received considerable interest in spine surgery applications. Ultrasound has many advantages over other imaging modalities. It has low cost, uses non-ionizing radiation, has a small footprint and a significantly shorter setup time in the OR. While iUS imaging is attractive for IGS, limited field of view and strong shadow artifacts induced by acoustic absorption of bones hinder its use in the clinical context for spine surgery. Instead, iUS scans are often used to collect anatomical features to register pre-operative CT or MR images to the operative field (Koo and Kwok, 2016; Wein et al., 2015; Rasoulian et al., 2012; Gill et al., 2012; Yan et al., 2012a).

In our previous work (Gueziri et al., 2019), we introduced a method for CT-to-iUS rigid registration of vertebra images that uses gradient orientation alignments. The gradients were sampled on the posterior surface of the vertebra located using a ray-tracing technique, which occupied over 80 % of the intra-operative processing time. In this paper, we extend out previous work and present an open-source platform for radiation-free pedicle screw navigation for open spine surgery. The platform provides a GPU-based implementation of CT-to-iUS rigid registration for rapid correction of patient-to-pre-operative image misalignments. We make the following contributions: 1) the correction of patient-to-pre-operative image misalignments is fully-automated and only involves a single iUS acquisition sweep during surgery; 2) we combine iUS image intensity in addition to gradient orientation alignment during registration to improve optimization convergence and robustness; 3) we obviate the need for the computation of posterior vertebral surface locations (i.e., bone segmentation), reducing the intra-operative pre-processing time; 4) we conducted thorough experiments on a porcine cadaver with multiple iUS scans and initial transform perturbations to assess the robustness of the registration in clinical conditions; and 5) we make the software publicly available for other groups to use. The results demonstrate that the proposed multi-metric optimization strategy significantly improves the robustness to large misalignments and provides a final registration that satisfies clinically accepted accuracy defined as 2 mm for spinal instrumentation (Cleary et al., 2000).

Related work

While many research papers have been published on CT-to-iUS registration, there is a lack of available IGS platforms that can be used for iUS-guided spine interventions and those that exist rely on 3D Slicer (Fedorov et al., 2012). For example, tracked iUS snapshots have employed for needle insertion (Ungi et al., 2012) and pedicle screw navigation (Ungi et al., 2013). The guidance was performed on ultrasound slices and a 3D rendering of CT volume can be added using manual registration. The use of a statistical model of the spine has been proposed to augment iUS images for needle insertion in 3D Slicer, using tracked (Khallaghi et al., 2010; Rasoulian et al., 2015) and tracker-less (Brudfors et al., 2015) ultrasound imaging. Statistical models provide anatomical data augmentation with-

out the need for pre-operative CT imaging, which is often the case for patients undergoing epidural injections. However, pathological variation in anatomy of the spine are not covered by such model-based approaches. For an exhaustive literature review, we refer interested readers to the recent survey of iUS-based image-guided spine interventions (Gueziri et al., 2020).

For most open spine interventions, the patient is placed in prone position and the posterior part of the vertebra is exposed during surgery. The vertebra surface is a good feature for rigid registration. Point-based registration methods are commonly used to obtain the CT-to-iUS transform, e.g., by minimizing the sum of distances between the posterior surface points extracted from iUS and the posterior surface points extracted from CT images. Using the Iterative Closest Point (Besl and McKay, 1992) algorithm, Muratore et al. (2002) reported an average target registration error (TRE) of 1.33 mm on a plastic phantom. A multi-vertebra registration framework was proposed by Nagpal et al. (2015), in which the Coherent Point Drift registration algorithm (Myronenko and Song, 2010) was used to align the points, achieving an average accuracy of 0.71-1.70 mm using clinical data. The CT images offer clear visibility of bony structures, facilitating vertebrae segmentation. However, this is not the case for iUS images. Bony tissues have a high acoustic impedance causing high response in ultrasound imaging. The surface of the vertebra appears hyperechoic followed by a signal drop off inducing shadow artifacts. Typically, the ultrasound response at a bone surface is 2–4 mm thick depending on the ultrasound beam penetration and inclination with respect to the bone surface (Jain and Taylor, 2004), with beams normal to the surface producing thinner responses. This causes the ultrasound intensity profile at the bone surface to be variable due to the shape of the vertebra. To reduce the effect of the segmentation noise and outliers on the registration accuracy, Rasoulian et al. (2012) proposed to use an unscented Kalman filter (Moghari and Abolmaesumi, 2007), to which a biomechanical regularization has been added to model the spine curvature. An average TRE of 2.2 mm was achieved on a sheep cadaver. Despite many efforts deployed to achieve accurate automatic iUS vertebral surface segmentation (Hacihaliloglu, 2017), the task is challenging and prone to errors affecting the final registration.

Alternatively, image-based registration approaches consist in optimizing a similarity metric that describes the CT-to-iUS alignment. To account for the intensity differences between the two modalities, Lang et al. (2012) proposed to simulate iUS slices from CT images. The similarity between the simulated and the real iUS images was obtained using linear correlation (Wein et al., 2008). Using a speckle-tracked ultrasound on a lumbar section of a lamb cadaver, the average TRE was 1.61-1.89 mm. Recently, Chan et al. (2020) reported a positional error of 1.2 mm $\pm$0.5mm and an angular error of $2.2^\circ \pm 2.0^\circ$ on a thoracic plastic phantom, using a Gaussian pyramid intensity registration. Segmented posterior surface images have been used to map both iUS and CT images into a common intensity space, in which cross-correlation (Yan et al., 2011; Koo and Kwok, 2016) and gradient orientation alignment (Gueziri and Collins, 2019; Gueziri et al., 2019) have been proposed to achieve the registration.

To obviate the need for iUS vertebra segmentation, Brendel et al. (2002) leveraged the hyperechoic response of the bone that produces bright intensities at the bone-tissue interface. They proposed to maximize the mean of iUS intensities that pass through the posterior surface of the vertebra on CT images. An improved version compensates for intensity loss due to depth to enhance bone surface visibility (Winter et al., 2008). The advantage of using the mean of iUS intensities (Brendel et al., 2002) is to reduce intra-operative pre-processing, such as vertebra segmentation, which is prone to errors and may require additional computation time. However, high bone reflectivity is modulated by the angle of incidence of the ultrasound beam when penetrating the bone tissue. In the proposed method, we combine the use of the mean of iUS intensities with gradient orientation alignment to take into account structural information present in both images.

Combination of intensity and gradient for registration is not new. Roche et al. (2001) used a correlation ratio metric which incorporates intensity and gradient information to register iUS images to MR brain images. In the context of spine registration, Chen et al. (2016) proposed a 2D-3D registration of iUS to CT images, in which a combination of gradient orientation and mutual information was used. The approach encodes the 2D orientation of the gradients in both iUS and CT slices. The orientation encoding is then used for estimating the probability density function used in a mutual information-like metric, named orientation code mutual information (OCMI). They reported an average TRE of 2.3 mm. There are three conceptual differences between our method and the one proposed by Chen et al. (2016): 1) in contrast to the OCMI in which the combination of intensity and gradient information is performed as a mutual information metric, we propose to use a linear combination of the two metrics improving computation efficiency and robustness of the registration; 2) while the OCMI approach uses local phase filtering of iUS images to enhance bone structures, our approach does not require pre-processing that increases the intra-operative computation time; and 3) in the OCMI approach, the gradient orientations are estimated in 2D images yielding a miscalculation of the image gradient in the out of plane direction. Consequently, there is no guarantee for the metric to be continuous, as small local changes may lead to large metric variability on highly curved edges. In our approach, the gradients are computed in the 3D reconstructed iUS and CT volumes to take into account the 3D orientation of the gradients that represent the complex shape of the vertebra.

Materials and methods

The system architecture is illustrated in Fig. 1. The registration and navigation features have been developed as a plugin for the Intraoperative Brain Imaging System (IBIS) navigation platform (Drouin et al., 2017). IBIS is a freely available platform that provides common functionalities used in IGS. It also allows rapid integration of new functionalities as plugins for specific applications. Data acquisition is achieved using the open-source Public software Library for Ultrasound (PLUS) (Lasso et al., 2014). The latter consists in a low-level interface library that allows the communication with a collection of devices commonly used in IGS. Prior to surgery, the posterior surface of the vertebra is segmented on the CT images using the forward-tracing method (Yan et al., 2011). During surgery, ultrasound images and tracking data are continuously sent to IBIS through the OpenIGTLink protocol (Tokuda et al., 2009). The registration takes place once the vertebra is exposed and ready to be instrumented. The open cavity is filled with saline solution to facilitate ultrasound propagation. IBIS iUS acquisition functionality is used to record a tracked iUS sequence. The role of the pedicle screw navigation plugin is two-fold: first, it provides patient-to-preoperative alignment using the iUS sequence and the segmented CT images; second, it allows real-time visualization of the predicted trajectory of the pedicle screw on reformatted axial and sagittal planes. Size and length of the pedicle screw can be adjusted to comply with the surgical plan. A demo video illustrating the entire navigation procedure on a Sawbones phantom is provided as supplementary material. The registration of CT to iUS images is a key step for accurate IGS navigation. In the following sections, we describe the proposed registration framework.

Registration framework overview

An overview of our registration framework is shown in Fig. 2. We use a similar iUS acquisition protocol to the one described in (Gueziri et al., 2019). The iUS scan consists in a single axial sweep along the caudo-cranial direction, starting from the inferior to the superior parts of the vertebra. Thus, the probe's trajectory forms a nearly linear path roughly along the midsagittal axis. Using the standard anatomical orientations of the CT scanner (i.e., Right-Anterior-Superior), we coarsely align the CT volume to the iUS volume without the need for additional manipulations to achieve an initial transformation. While additional sweeps would provide more informa-

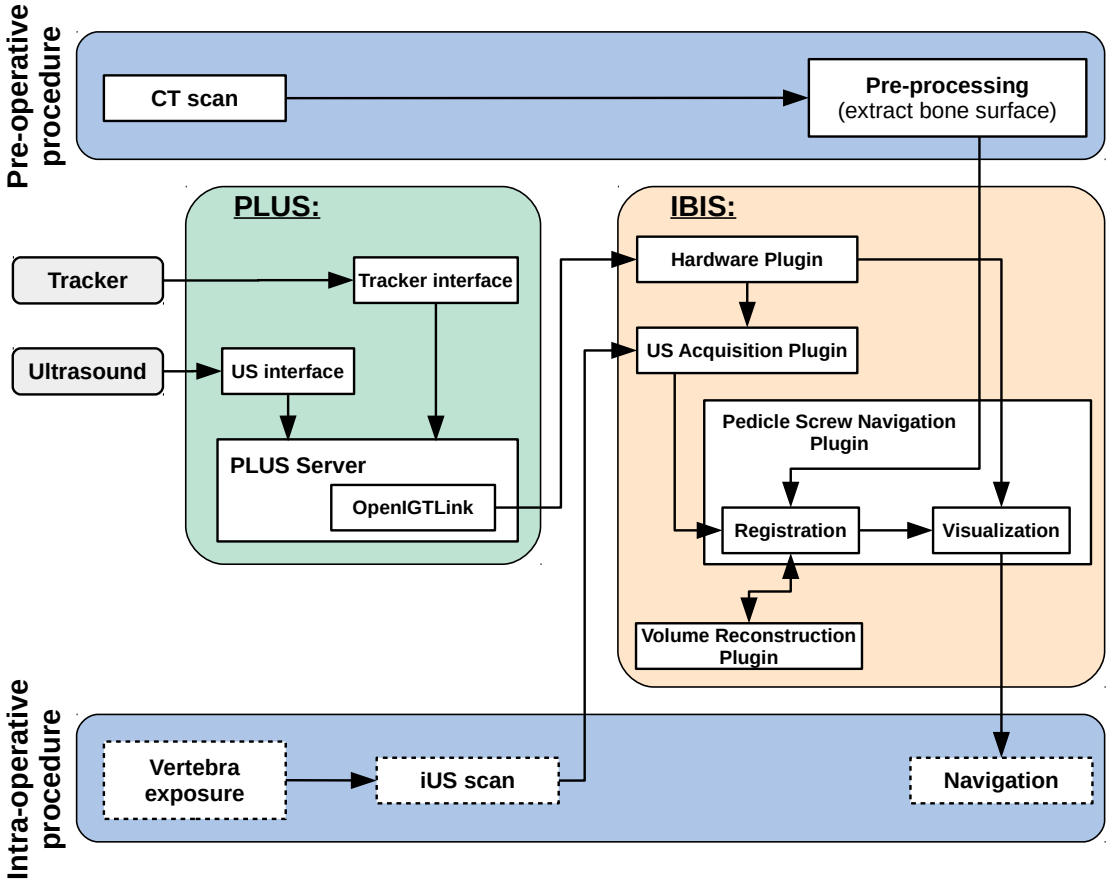

Figure 1: System architecture of the CT-to-iUS rigid registration framework. Doted boxes indicate the intra-operative procedure required to be achieved by the surgeon.

tion in the iUS volume that can be used during registration, the motivation behind the proposed protocol is its ease of use in a clinical environment. Considering an open-back surgery, in which the spinous process and the laminae of the vertebra are exposed, the ultrasound signal attenuation is low as it propagates in a saline solution compared to muscle and fat tissues present in a percutaneous scan. The surface of the laminae is orthogonal to the probe's orientation yielding a strong ultrasound response. This allows the scan to capture sufficient features to achieve the registration. To minimize intra-operative computation time, the iUS volume reconstruction is performed on the GPU (Drouin et al., 2017). Starting from this initial alignment, a multi-metric optimization strategy is performed to refine the registration. During the optimization, the CT to iUS alignment match is evaluated using two metrics: gradient orientation alignment and mean of iUS intensities.

Gradient orientation alignment metric

Given the hyperechoic appearance of the bone surface in iUS images, one can expect a strong gradient where ultrasound beams are normal to the vertebral surface. Consequently, these points are good candidates to be evaluated for gradient orientation alignment (see Fig. 3). Similarly, a strong gradient is obtained from the segmented CT image along the posterior surface of the vertebra. De Nigris et al. (2012) showed that the registration can be improved by evaluating gradient orientation alignment at selected locations sampled from the iUS image. Therefore, only the gradients having a magnitude above the 80^{th} percentile are selected (as suggested in (De Nigris et al., 2013)).

The first step of the gradient alignment metric consists in computing the image gradients of

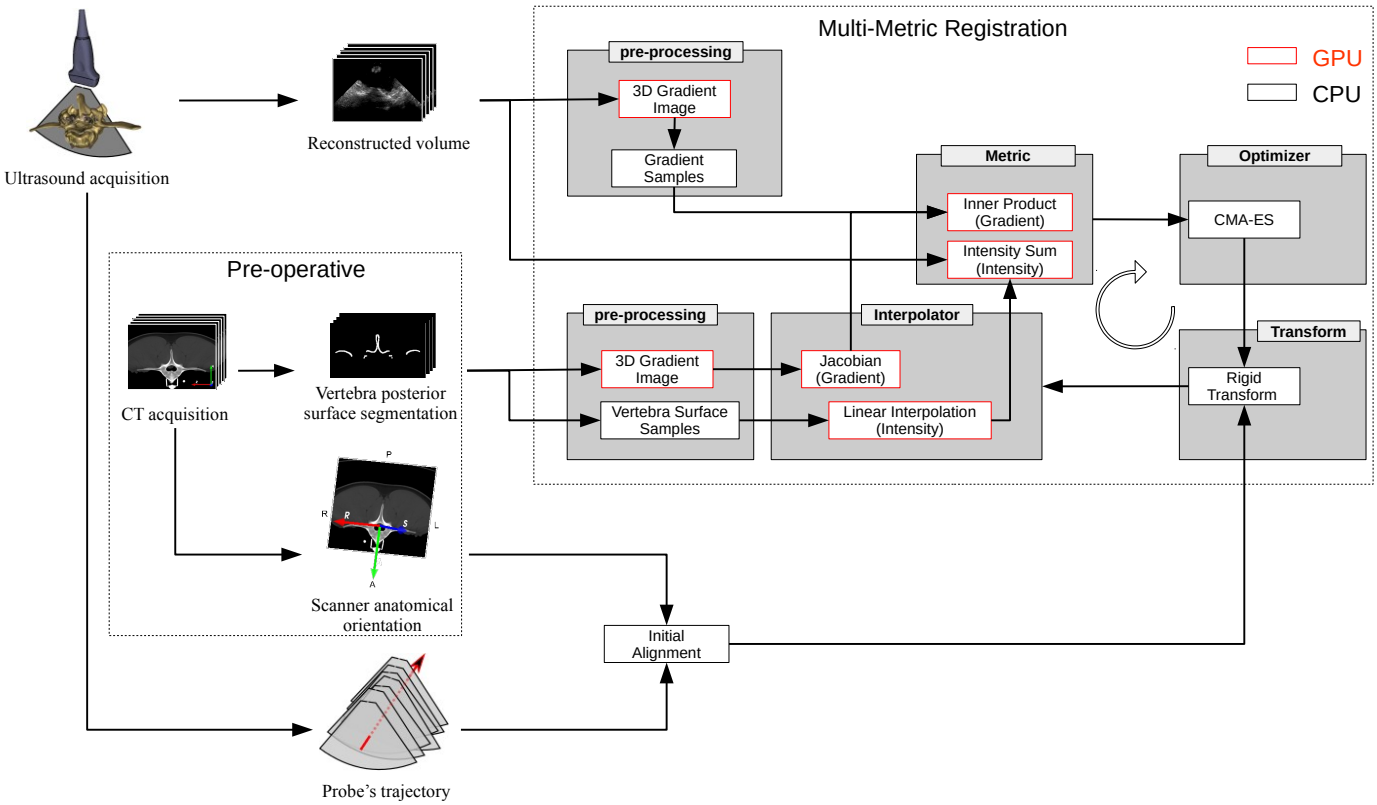

Figure 2: Flowchart of the proposed registration method.

CT and iUS images. Let ∇I_{CT} denotes the image gradients of the CT segmented moving image and ∇I_{US} denotes the image gradients of the iUS fixed image. Then, candidate gradients are sampled from the iUS image gradients ∇I_{US}. For computation efficiency, gradient images are computed on the GPU by convolving the original images with a Gaussian derivative operator. At each iteration of the optimization, the gradient orientation alignment at a given location $\mathbf{x}$ is measured as

$$S_G\Big(\nabla I_{\mathrm{US}}(\mathbf{x}), \nabla I_{\mathrm{CT}}(\mathbf{T}(\mathbf{x}))\Big) = \left\langle \frac{\nabla I_{\mathrm{US}}(\mathbf{x})}{|\nabla I_{\mathrm{US}}(\mathbf{x})|}, \frac{\nabla I_{\mathrm{CT}}(\mathbf{T}(\mathbf{x}))}{|\nabla I_{\mathrm{CT}}(\mathbf{T}(\mathbf{x}))|} \right\rangle^n, \quad (1)$$

where $\mathbf{T}(\mathbf{x})$ is the transformed location of $\mathbf{x}$, $\langle ., . \rangle$ denotes the inner product operator and $n \in \mathbb{N}$ is a free parameter which characterizes the matching criterion and was set to $n = 64$ as suggested in (De Nigris et al., 2013).

To avoid recomputing the moving CT image at each transformation update, the transformed moving image gradient is estimated using the transposed spatial Jacobian matrix of the transform $J^T_{\mathbf{T}(\mathbf{x})}$ and the original CT image gradient $\nabla_{\mathbf{T}} I_{\mathrm{CT}}(\mathbf{T}(\mathbf{x}))$, such that

$$\nabla I_{\mathrm{CT}}(\mathbf{T}(\mathbf{x})) = J^T_{\mathbf{T}(\mathbf{x})} \cdot \nabla_{\mathbf{T}} I_{\mathrm{CT}}(\mathbf{T}(\mathbf{x})). \quad (2)$$

Since the evaluation of the metric is performed on a limited number of sampled locations (i.e., $|\nabla I_{\mathrm{US}}| > 80^{\mathrm{th}}$ percentile), the computation of the metric is highly efficient.

Mean of iUS intensities metric

Because of the high iUS intensity response along the vertebral surface, when registered, the surface of the vertebra segmented on the CT image passes through high iUS intensities. The mean of iUS intensities on vertebral surface points defined by CT is maximized when the iUS data is registered with the CT volume. The metric is given by

$$S_I\Big(I_{\mathrm{US}}(\mathbf{x}), I_{\mathrm{CT}}(\mathbf{T}(\mathbf{x}))\Big) = I_{\mathrm{US}}(\mathbf{x}) \cdot I_{\mathrm{CT}}(\mathbf{T}(\mathbf{x})), \quad (3)$$

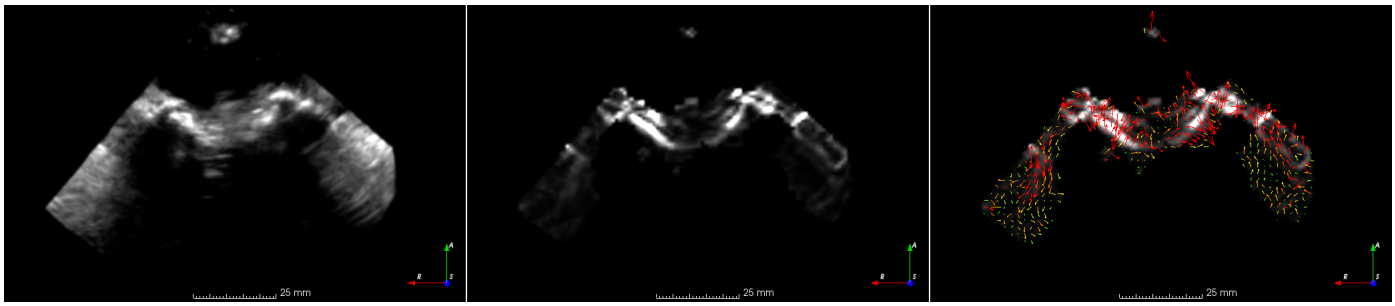

Figure 3: Axial slice of a reconstructed ultrasound volume of a vertebra: intensity image (left), gradient magnitude (middle), and gradient vectors (right). Note that the gradients are computed on the 3D ultrasound volume.

where $I_{\mathrm{CT}}(\mathbf{x})$ corresponds to the binary segmentation of the vertebra surface of the CT image. Subsequently, only intensities along the vertebra surface segmented on CT are considered during the computation. Because $\mathbf{x}$ points are sampled from the CT space, Eq 3 can be rewritten as

$$S_I\Big(I_{\mathrm{US}}(\mathbf{x}), I_{\mathrm{CT}}(\mathbf{T}(\mathbf{x}))\Big) = I_{\mathrm{US}}(\mathbf{T^{-1}}(\mathbf{x})) \qquad (4)$$

Note that the iUS intensities are normalized. Therefore, Eq 4 yields values ranged within $[0, 1]$.

Optimization

Let ϕ be the translation and rotation parameters of the rigid transform $\mathbf{T}$. To optimize for ϕ, we used the covariance matrix adaptation evolution strategy (CMA-ES) (Hansen and Ostermeier, 2001) as it has been shown to provide good results for rigid vertebra registration (Winter et al., 2008). The optimized metric S is a linear combination of the gradient orientation alignment and the mean of iUS intensities along the vertebra surface, such that

$$\begin{aligned} &S(I_{\mathrm{US}}, \mathbf{T}(I_{\mathrm{CT}}, \phi)) = \\ &\lambda \left[\frac{1}{|\Omega_{\mathrm{US}}|} \sum_{\mathbf{x}\in\Omega_{\mathrm{US}}} S_G\Big(\nabla I_{\mathrm{US}}(\mathbf{x}), \nabla I_{\mathrm{CT}}(\mathbf{T}(\mathbf{x}))\Big)\right]^{\frac{1}{n}} + \\ &(1-\lambda)\left[\frac{1}{|\Omega_{\mathrm{CT}}|} \sum_{\mathbf{x}\in\Omega_{\mathrm{CT}}} S_I\Big(I_{\mathrm{US}}(\mathbf{x}), I_{\mathrm{CT}}(\mathbf{T}(\mathbf{x}))\Big)\right], \end{aligned} \qquad (5)$$

where $\mathbf{T}(I_{\mathrm{CT}}, \phi)$ denotes the transformed CT image, Ω_{US} is the set of selected iUS samples satisfying gradient magnitude selection criterion, Ω_{CT} is the set of samples lying on the CT posterior surface of the vertebra and λ a hyperparameter balancing the two metrics. Note that the gradient orientation alignment metric in Eq. 1 yields small values when n is large. Therefore, the term $\frac{1}{n}$ is used in Eq. 5 to normalize the metric values. Note that powering the gradient term to $\frac{1}{n}$ does not affect the metric sensitivity to gradient misalignment as discussed in (De Nigris et al., 2012). This is because the normalization term is globally applied to the metric after the summation of the gradient's dot products in order to match the iUS mean of intensities metric. Eq. 5 accounts for gradient orientation misalignment of strong structures present on the images and the misalignment of the visible vertebral surface. Finally, the registration transform is obtained by

$$T^{\mathrm{reg}} = \arg\max_{\phi} S(I_{\mathrm{US}}, \mathbf{T}(I_{\mathrm{CT}}, \phi)). \qquad (6)$$

Visualization

Once the registration completed, the surgeon can navigate using a pointer-like tracked instrument, e.g., a stylus, a pedicle probe or a drill. During screw insertion, high complication risks are often associated with medial and anterior breaches, which can be assessed post-operatively using X-ray or CT imaging. Breaches are inspected by visualizing axial and sagittal views of the screw passing through bone anatomy. To highlight the predicted trajectory of the insertion intra-operatively, a similar visualization technique is used, in which axial and sagittal views are reformatted to match the pointer's orientation (Fig. 4). Specifically, during navigation, each

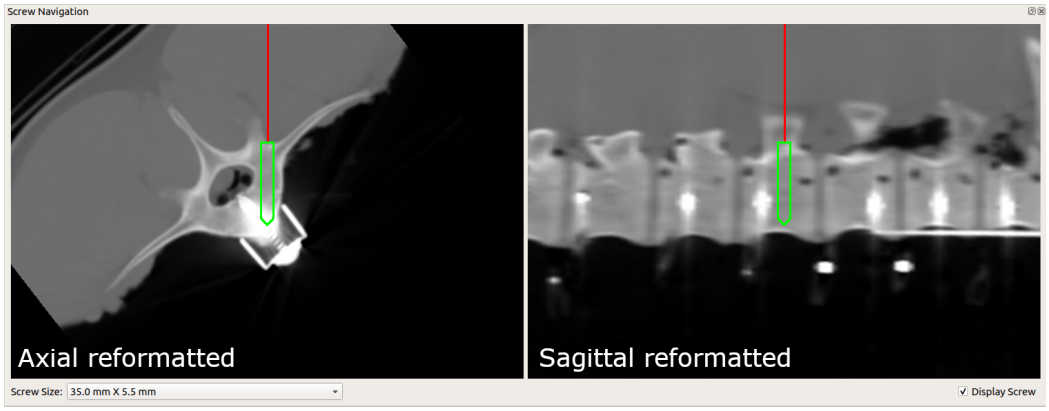

Figure 4: Graphical window interface for pedicle screw navigation with reformatted axial and sagittal views: tracked instrument (red), screw cross-section (green), screw length 35 mm and screw diameter 5.5 mm.

view follows the instrument's axial (or sagittal) orientation and the CT slice associated with this view is recomputed in real-time. A cross-section of the screw is displayed at the tip of the instrument indicating the current trajectory. The screw length and diameter can be modified to correspond to the desired depth and pedicle width, to prevent anterior and lateral breaches, respectively.

Implementation

Algorithm 1 outlines the implementation details of the method. Note that lines 16 and 21 are performed on GPU threads, which allows both gradient orientation alignment and mean of iUS intensity metrics to be efficiently computed in parallel. The algorithm was implemented in C++ based on the registration framework used in the Insight Segmentation and Registration Toolkit (ITK) (Yoo et al., 2002). In addition, the Elastix (Klein et al., 2010) was used for the CMA-ES optimization and the OpenCL library (Stone et al., 2010) for GPU computing. The source code is freely available on GitHub (`https://github.com/IbisNeuronav/Ibis`). All computations were performed using an Intel© Core™ i7-3820 CPU at 3.6 GHz × 8 station and a NVIDIA GeForce GTX 670 graphics card with 4 Gb of memory.

We conducted a pilot experiment (similar to one described in Section *Experiment 2: Robustness to initial alignment*), in which 3 vertebral levels were involved and λ was varied from 0.1 to 0.9 by increments of 0.1. For each vertebra, 10 registration trials were performed. The initial registration transform was obtained by performing a probe's trajectory alignment followed by a random misalignment within ± 15 mm translation and $\pm 10°$ rotation. We observed comparable results when λ is in the range $[0.4, 0.8]$. The registration behaviour tends towards gradient orientation alignment when $\lambda > 0.8$ and towards mean of iUS intensities when $\lambda < 0.4$. We did not observe any abnormal registration behaviour with the variation of the parameter. In all of our experiments, we empirically set $\lambda = 0.7$.

Other parameters that may influence the registration outcomes are: the percentile of gradient magnitude, the resolution of the iUS volume, the resolution of CT volume, the thickness of the posterior vertebra surface, and the parameters for the CMA-ES optimizer. Here, we briefly discuss the setting of each parameter. The percentile of gradient magnitude used to select gradient samples was set to 80^{th} percentile based on the original work by De Nigris et al. (2013). The choice of the parameter's value is related to the quality of the iUS images, and more specifically how clear the bone surface appears on iUS images. When the contrast produced by the bone surface is high, values over or equal to 80 % tend to isolate good gradient candidates for the registration. On the other hand, on images where the bone surface intensity is not prominent (e.g., due to signal absorption/loss of posterior muscles or high bone penetration), a lower threshold is recommended to allow gradient

Algorithm 1 Pseudo-code for the proposed multi-metric registration approach.

Input: I_{US}, /* iUS reconstructed volume */
I_{CT}, /* segmented CT volume */
λ /* metric balance parameter */
Output: $\mathbf{T}^{\text{reg}}$: registration transform
/* Gradient orientation */
$G_{\text{US}} \leftarrow \text{gradient}(I_{\text{US}})$
$G_{\text{CT}} \leftarrow \text{gradient}(I_{\text{CT}})$
$t_{\text{US}} \leftarrow \text{percentile}(G_{\text{US}}, 0.8)$
$\Omega_{\text{US}} \leftarrow \text{sample}(G_{\text{US}}, t_{\text{US}})$
Load G_{CT} and Ω_{US} on GPU
/* Mean of iUS intensities */
$\Omega_{\text{CT}} \leftarrow \text{sample}(I_{\text{CT}})$
Load I_{US} and Ω_{CT} on GPU
/* Probe's trajectory alignment */
/* (see (Gueziri and Collins, 2019)) */
$\{\mathbf{x}^{\text{US}}_{\text{mass}}, \mathbf{x}^{\text{US}}_{\text{distal}}, \mathbf{x}^{\text{US}}_{\text{sup}}\} \leftarrow$ probe_trajectory
$\{\mathbf{x}^{\text{CT}}_{\text{mass}}, \mathbf{x}^{\text{CT}}_{\text{distal}}, \mathbf{x}^{\text{CT}}_{\text{sup}}\} \leftarrow \text{scanner\_RSA}(I_{\text{CT}})$
$\mathbf{T}^{\text{init}} \leftarrow \arg\min_{\mathbf{T}} \sum_i ||\mathbf{T}(\mathbf{x}^{\text{CT}}_{\mathbf{i}}) - \mathbf{x}^{\text{US}}_i||$
$\mathbf{T} \leftarrow \mathbf{T}^{\text{init}}$
/* Optimization */
$\phi \leftarrow \text{get\_transform\_parameters}(\mathbf{T})$
while stop condition not met **do**
  $m_G \leftarrow 0$
  for $\mathbf{x} \in \Omega_{\text{US}}$ **do** /* Parallel GPU thread */
    $m_G \leftarrow m_G + \langle G_{\text{US}}(\mathbf{x}), G_{\text{CT}}(\mathbf{T}(\mathbf{x}))\rangle^n$
  end for
  $S_G \leftarrow \left(\frac{m_G}{|\Omega_{\text{US}}|}\right)^{\frac{1}{n}}$
  $m_I \leftarrow 0$
  for $\mathbf{x} \in \Omega_{\text{CT}}$ **do** /* Parallel GPU thread */
    $m_I \leftarrow m_I + I_{\text{US}}(\mathbf{T^{-1}}(\mathbf{x}))$
  end for
  $S_I \leftarrow \frac{m_I}{|\Omega_{\text{CT}}|}$
  $S = \lambda S_G + (1-\lambda) S_I$
  $\phi \leftarrow \text{update}(\phi, S)$
  $\mathbf{T} \leftarrow \text{calculate\_transform}(\phi)$
end while
$\mathbf{T}^{\text{reg}} \leftarrow \mathbf{T}$

sampling on regions with moderate contrast. The iUS volume resolution was set to $1 \times 1 \times 1\,\text{mm}^3$. In our previous work (Gueziri et al., 2019), we investigated different reconstructed iUS volume resolutions varying between $0.5 \times 0.5 \times 0.5\,mm^3$ and $1.5 \times 1.5 \times 1.5\,\text{mm}^3$ using gradient orientation registration. While the computation time increases with finer resolution, no significant impact on the accuracy was observed. The resolution and slice thickness of the CT volume were fixed to $0.35 \times 0.35\,\text{mm}^2$ and 2 mm, respectively. The effect of different parameters of the CT scan has not been investigated in this study. The thickness of the posterior vertebral surface extracted from CT images was set to 2 mm based on the work by Yan et al. (2011). A typical value range is 1–3 mm and depends on the CT image resolution. A too small value produces a discontinuous surface, while a too large value may result in a decrease of registration accuracy. Finally, parameters affecting the convergence of the CMA-ES optimizer can be modified through the advanced options of the graphical user interface. Table 1 summarizes a list of recommended values for each parameter.

Experiment

Porcine data

Porcine lumbar spines are frequently used as an alternative to human specimens for spinal instrumentation as they share some similar anatomical and functional properties (Dath et al., 2007; Sheng et al., 2010). A lumbosacral section of a porcine cadaver was obtained from a certified local butcher. The specimen presents 7 vertebral levels (T15 to L6) and was scanned with a PQ6000 CT scanner (Picker International Inc., Cleveland, OH, United States). Superior to inferior axial slices were acquired in supine position. The CT acquisition has been done following the preoperative spine neurosurgery protocol at the Montreal Neurological Institute and Hospital. Typically, CT imaging is performed with bone enhancement calibration and a slice thickness of 2 mm, unless otherwise required by the surgeon. In this study, we are interested in single vertebra alignment in order to assess the quality of the proposed registration approach without introducing errors related to the spine curvature. Therefore, the CT volume was manually divided into sub-volumes, each one containing a single vertebra.

The iUS acquisitions were collected using a HDI 5000 ultrasound with a phased array probe P4-7 (Philips, Amsterdam, Netherlands) and an optical tracking camera (Polaris, Northern Digital Inc., ON, Canada) was used to track the probe. Ultrasound probe calibration was performed using a N-shaped wire phantom (Drouin et al., 2017). The phantom consists in 4 planes of N-shaped wires. When intersecting with the ultrasound plane, each N-shaped wire creates points on the ultrasound image that are manually identified by

Parameters	Recommended value(s)	Description
λ	0.4 – 0.8	Large values emphasize gradient orientation Small values emphasize mean iUS intensities
Gradient sampling (percentile)	80^{th} percentile	Decrease for low contrasted bone surface
iUS volume resolution	$0.5 \times 0.5 \times 0.5\,\text{mm}^3$ to $1.5 \times 1.5 \times 1.5\,\text{mm}^3$	Finer is better, but increases computation time
CT vertebral surface thickness	1–3 mm	Decrease for high CT resolution
CMA-ES optimizer (Hansen and Ostermeier, 2001)	Population size: 60 Max iterations: 300 Initial σ: 1 Tolerance: 0.0001	Number of samples generated per iteration Maximum number of iteration The initial standard deviation used to generate offspring Tolerance value for convergence

Table 1: Summary of and recommended values for parameters that can influence the registration results.

the operator on IBIS. Because the geometry of the N-shaped wires is known the calibration matrix is estimated by establishing the correspondence between the ultrasound image coordinate points and world coordinate points. Accuracy of the calibration was measured using a second cross-wire phantom and varies between 0.49 mm and 0.82 mm (Mercier et al., 2011).

For each vertebra, three iUS scans were acquired: $\text{iUS}_{\text{centered}}$, a caudo-cranial transverse scan centered on the spinous process, iUS_{left}, a caudo-cranial transverse scan 1 cm to the left of the spinous process, and $\text{iUS}_{\text{right}}$, a caudo-cranial transverse scan 1 cm to the right of the spinous process. The iUS volume is reconstructed by averaging a Gaussian distance weighted intensity for each voxel inside a 2 mm search radius.

The navigation system was operating on the IBIS platform. Using bone-implanted fiducial markers, a ground truth registration transform was obtained for each vertebra. Each fiducial consists in a plastic pipette containing a metallic sphere visible on CT images. Pre-operatively, the coordinates of the sphere centers on CT images were obtained using a threshold segmentation. Intra-operatively, before ultrasound scan, the patient coordinates of each fiducial were measured using a tracked pointer. Then, a pair-wise point correspondence between both set of points was employed to determine the ground truth registration. To validate the quality of the ground truth and account for inter-operator manipulation errors, measurements of the fiducial in patient coordinate space were repeated 50 times, yielding a median fiducial registration error (FRE) of 0.452 mm and an interquartile range (IQR) of 0.122 mm. In addition, 20 anatomical landmarks were manually identified on the CT image and used to compute the target registration error (TRE) of the 50 repetitions. The median TRE was 0.718 mm and the IQR was 0.462 mm (Yan et al., 2012b). The reported target registration error (TRE) was measured on 7 anatomical points located on the vertebra surface, corresponding to the apex of the spinous process, left and right laminae, left and right superior articular processes and left and right inferior articular processes. We define the success rate (SR) as the proportion of registrations achieving a TRE below 2 mm as suggested by Cleary et al. (2000) for lumbar spine intervention.

Experiment 1: Clinical setup

In order to evaluate our method, we compared three variants of the proposed metric: (G) using only gradient orientation alignment metric, (I) using only mean of iUS intensities metric, and (G+I) the proposed combined metric Eq. 5. The experiment aims at evaluating the proposed registration framework for a clinical setup. For each iUS acquisition, the 7 vertebral levels were registered individually using the iUS probe's trajectory initial alignment followed by the multi-metric registration. The CMA-ES optimizer is non-deterministic and yields slightly different results at each registration runtime. To account for stochastic convergence variability, the registration trials were repeated 100 times for each vertebra. A total of 2,100 trials were performed for each metric condition (3 iUS acquisitions $\times$ 7 vertebral levels $\times$ 100 repetition).

Figure 5 shows qualitative registration results obtained with L4. The overall accuracy and computation time results are summarized in Table 2. With the suggested sweep, $\text{iUS}_{\text{centered}}$, the proposed (G+I) metric resulted in a registration TRE below 2 mm for all vertebral levels (Figure 6), yielding 100 % success rate and a median TRE of 1.47 mm. The success rate of the registrations is the highest when using the (G+I) metric for all the iUS acquisitions ($\text{SR}_{(\text{G+I})} = 89.86\,\%$ for iUS_{left} and $\text{SR}_{(\text{G+I})} = 88.57\,\%$ for $\text{iUS}_{\text{right}}$). The accuracy obtained using only the gradient orientation alignment on the centered acquisition ($\text{TRE}_{(\text{G})} = 1.20$ mm) decreases when using left and right acquisitions ($\text{TRE}_{(\text{G})} = 1.97$ mm and $\text{TRE}_{(\text{G})} = 1.99$ mm, respectively), highlighting a lack of robustness owing to partial visibility of the vertebra in iUS images. A repeated-measure analysis of variance (ANOVA) (Chambers and Hastie, 1992) reveals a statistically significant effect of the registration method on the TRE value ($F_{2,12} = 8.01, p = 0.006$). Specifically, post hoc pair-wise comparisons using the Tukey HSD test with Bonferroni correction indicated a significant difference between the gradient (G) and the combination (G+I) metrics ($p < 0.001$), but the difference was not statistically significant between intensity (I) and combination (G+I) metrics ($p = 0.056$), nor between intensity (I) and gradient (G) metrics ($p = 0.31$).

The TRE results obtained with the combination (G+I) metric outperforms the results reported in (Yan et al., 2012b) and are comparable to ones reported in (Gueziri et al., 2019) on the same dataset. The results are comparable to other state-of-the-art methods reporting TRE on animal experiments: 1.48 mm (in 116 s) (Yan et al., 2012a) and 2.18 mm (in 100 s) (Koo and Kwok, 2016) on a porcine cadaver, 2.2 mm (in 29 min) (Rasoulian et al., 2012) and 0.62-2.26 mm (in 43 min) (Gill et al., 2012) on a sheep cadaver, and 1.61 mm (in 15–30 min) (Lang et al., 2012) on a lamb cadaver. However, our parallel GPU implementation allows a highly effective metric computation. The registration time is not severely affected when combining both metrics ($\text{Time}_{(\text{G})} = 5.57$ s, $\text{Time}_{(\text{I})} = 5.25$ s and $\text{Time}_{(\text{G+I})} = 6.62$ s). Note that the high computation time in (Rasoulian et al., 2012) and (Gill et al., 2012) involves multiple vertebrae registration, which can not be directly compared to a single vertebra registration. The time required for the initial alignment using the probe's trajectory is negligible (0.05 s on average).

Experiment 2: Robustness to initial alignment

A second experiment was carried out to assess the robustness of the multi-metric registration method to initial misalignment. In this experiment we consider the transverse centered iUS acquisition, $\text{iUS}_{\text{centered}}$. For each vertebral level, 100 initial *misalignments* were generated by adding a random rotation followed by a random translation to perturb the initial probe trajectory-based transform. The random translation and rotation were respectively sampled from a uniform distribution bounded within $[-20\,\text{mm}, 20\,\text{mm}]$ and $[-20°, 20°]$ in every spatial direction. Table 3 shows median TRE and success rates obtained for each vertebral level. The combination of gradients and intensities metric (G+I) yields the best robustness to initial misalignment with an average success rate of 83.14 %. Because the success rate represents a categorical dependent variable (i.e., 1 if the TRE is below 2 mm and 0 otherwise), a generalized logistic regression model (McCullagh and Nelder, 1989; Bates, 2005) was considered to analyze the statistical significance of the difference in robustness results. Similar to the repeated measure ANOVA carried out in the first experiment, the registrations obtained for each vertebral level are considered to be correlated. This is expected as the registration error is relative to the ground truth transform for each vertebral level. Therefore, in our model, we consider the vertebral level to be a random effect and the registration method to be a fixed effect with variable average deviations across vertebral level (Quené and van den Bergh, 2008). Considering the combination (G+I) metric as the baseline (i.e., the intercept refers to the combination metric in the linear model), we found a statistically significant difference in success rate results ($p < 0.01$), with odds ratios $\text{OR}_{(\text{G+I})} = 7.37$, $\text{OR}_{(\text{G})} = 3.58$ and

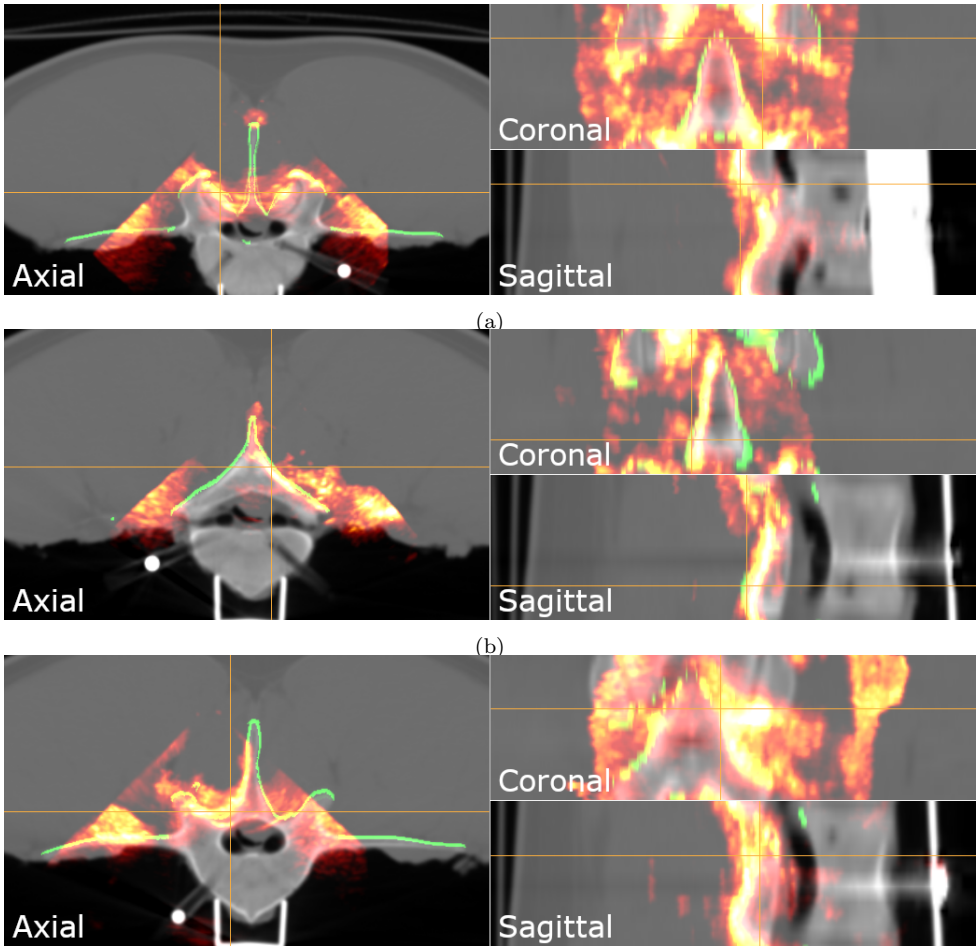

Figure 5: Qualitative registration results of L4: (a) centered acquisition, (b) left acquisition and (c) right acquisition. Ultrasound intensities are displayed in *hot* color map and posterior surface of the vertebra is highlighted in green.

$\mathrm{OR}_{(\mathrm{I})} = 0.07$, for the combination, gradient and intensity metrics respectively.

Figures 7a and 7b show histogram distribution of the final TRE. The combination metric (G+I) shows the highest population of TREs that are below the clinical acceptance threshold. For the intensity metric (I) and the combination metric (G+I), the TREs of the trials that failed registration are significantly higher with a median TRE of $\mathrm{TRE}_{(\mathrm{I})} = 17.90\,\mathrm{mm}$ (IQR $= 28.31\,\mathrm{mm}$) and $\mathrm{TRE}_{(\mathrm{G+I})} = 29.15\,\mathrm{mm}$ (IQR $= 10.17\,\mathrm{mm}$). This could be due to the optimization converging to a local maximum or failing the convergence. On the other hand, registration failures using the gradient metric (G) have a lower median TRE of $3.24\,\mathrm{mm}$ (IQR $= 23.28\,\mathrm{mm}$), which may indicate difficulties of the optimizer to locate the global maximum. To analyze the effect of the initial misalignment on the registration accuracy, density scatter plots of the final TRE according to the initial TRE generated from the random initialization are shown in Figs. 7c and 7d. Increasing the TRE of the initial misalignment does not seem to be linearly correlated with the loss of registration accuracy (Pearson's correlations $r_{(\mathrm{G})} = 0.21$, $r_{(\mathrm{I})} = 0.19$ and $r_{(\mathrm{G+I})} = 0.17$).

To gain more insight into how the proposed metric behaves with respect to local image misalignment, we monitored the metric values as the iUS and CT images are being gradually misaligned. Starting from the ground truth transform, we incrementally apply a 0.05 mm translations in every direction and measure (G), (I) and (G+I) metrics. Similarly, the metrics are monitored with an incremental rotation transform of 0.05° in every direction. The total range of

	Method	TRE (mm) median	TRE (mm) IQR	Success rate (%)	Time (s) Reconstruction	Time (s) Registration	Time (s) Total
$iUS_{centered}$	Gradient (G)	**1.20**	0.66	85.14	1.84	3.73	5.57
	Intensity (I)	1.50	0.92	71.43	1.94	3.31	5.25
	Combination (G+I)	1.47	0.39	**100**	1.93	4.69	6.62
	Yan et al. (2012b)	1.93	0.72	–	–	–	∼120
	Gueziri et al. (2019)	1.48	0.68	84.42	–	–	10.79
iUS_{left}	Gradient (G)	1.97	0.72	53.57	1.99	3.89	5.87
	Intensity (I)	**1.44**	1.01	71.57	1.99	3.33	5.33
	Combination (G+I)	1.63	0.78	**89.86**	1.97	5.11	7.07
	Yan et al. (2012b)	2.31	1.17	–	–	–	∼120
	Gueziri et al. (2019)	1.69	0.63	71.42	–	–	11.63
iUS_{right}	Gradient (G)	1.99	0.59	50.57	2.18	4.15	6.34
	Intensity (I)	1.23	1.00	71.43	2.19	3.34	5.53
	Combination (G+I)	**1.21**	0.57	**88.57**	2.19	5.21	7.39
	Yan et al. (2012b)	1.93	1.38	–	–	–	∼120
	Gueziri et al. (2019)	1.70	0.78	68.4	–	–	10.58

IQR: interquartile range.

Table 2: Registration accuracy and computation time results for each iUS acquisition. Best TREs and success rates are indicated in bold.

Level	Gradient TRE (mm)	Gradient SR (%)	Intensity TRE (mm)	Intensity SR (%)	Combination TRE (mm)	Combination SR (%)
T15	1.03 (20.84)	52	30.39 (8.02)	22	22.55 (35.12)	43
L1	2.61 (0.39)	3	2.45 (23.27)	0	1.76 (0.20)	77
L2	1.11 (0.18)	93	1.50 (0.01)	92	1.20 (0.04)	92
L3	1.80 (0.20)	93	1.31 (0.03)	93	1.57 (0.09)	96
L4	1.13 (0.18)	92	1.50 (0.03)	76	1.37 (0.03)	84
L5	1.22 (0.56)	94	1.18 (0.02)	88	1.16 (0.03)	97
L6	1.06 (0.36)	80	2.26 (0.03)	0	1.54 (0.24)	93
All	1.27 (1.24)	72.43	1.70 (1.13)	53.00	1.52 (0.52)	83.14

TRE: median target registration error (interquartile range), SR: success rate.

Table 3: Registration accuracy results for probe's trajectory misalignment within ±20 mm translation and ±20° rotation.

transformations was $[-10\,\text{mm}, 10\,\text{mm}]$ in translation and $[-10°, 10°]$ in rotation. Figure 8 shows the results of each metric obtained with all vertebrae. Note that the metric values are centered by subtracting the mean to facilitate comparison. Despite the flattened shape of the gradient metric (G) curve, the median global maximum (blue line) approximates the ground truth (black line). The intensity metric (I) has a smoother curve. While the translation variations resulted in a curve with a narrow width favoring optimization of the global maximum, the curve obtained from rotation variations is wider with a less accurate global maximum. The combination metric (G+I) takes advantage of both metrics: 1) it reduces the noise of the gradient metric (G) curve resulting in a smoother curve while preserving the global shape of the intensity metric (I). The global maximum of the (G+I) lies somewhere between the peak of the (G) curve and the peak of (I) curve. The hyperparameter λ acts as a trade-off between the shape of the two curves, such as increasing λ results in a metric behaving like the gradient orientation alignment (G) whereas decreasing λ would force the metric to behave like mean of iUS intensities (I).

Discussion

The quality of the iUS acquisition may have a significant impact on the quality of the registration. In a clinical condition, parts of the anatomy may be missing on the iUS scan. Experiments on a porcine cadaver demonstrated that our iUS-based registration framework achieved a success rate of 100 % with the proposed caudo-cranial iUS acquisition protocol, and showed a high robustness to missing anatomy with success rates of 89.86 % and 88.57 % achieved using left and right shifted acquisitions, respectively. In addi-

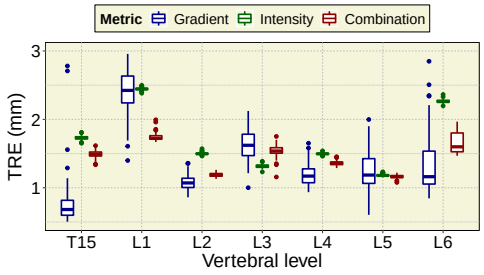

(a)

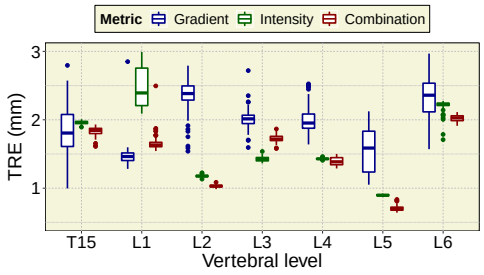

(b)

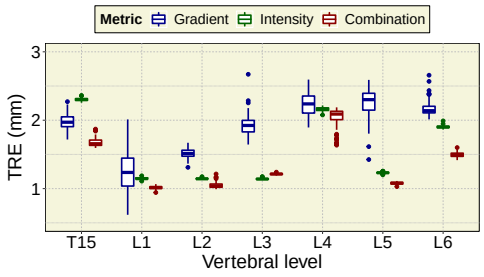

(c)

Figure 6: Boxplot of the target registration error for all vertebral levels: (a) centered acquisition, (b) left acquisition and (c) right acquisition.

tion, the approach showed low sensitivity to initial misalignment as no correlation was found between the initial misalignment error and the final registration error. This is important as during surgery, the iUS acquisitions are expected to be captured by the surgeon, whose level of expertise with ultrasound imaging may be variable. The one-sweep caudo-cranial acquisition protocol reduces the burden of intra-operative imaging, and yields 100 % success rate for registration. It is important to note that the caudo-cranial sweep is only used to establish an initial alignment. During registration, the metric is optimized based on the reconstructed iUS volume. Hence, one can consider doing a first caudo-cranial sweep (for alignment) followed by arbitrary scans that can be merged to reconstruct an iUS volume with more information (for registration). While this feature is not yet available in our platform, the approach is being investigated as potential future work. The high success rate of 83.14 % obtained when randomly perturbing the probe's trajectory alignment of up to ±20 mm translation and ±20° rotation highlights the robustness of our proposed registration framework to the iUS acquisition conditions. In addition, the registration is performed under 8 seconds of processing time, including ∼ 2 s to reconstruct the iUS volume and ∼ 6 s to align the images. This leverages the real-time functionality of ultrasound to perform frequent correction of the patient misalignment during surgery. In the case of unsatisfactory acquisition or initial alignment, most of the registration failures were visually identifiable as the resulting TRE was significantly large (over 20 mm), which provides the surgeon with the option of quickly re-acquiring additional iUS scans.

In addition to iUS image quality, artifacts affecting preoperative CT images influence the overall navigation accuracy. Partial volume artifacts, metal artifacts, image distortion and pathological factors, decrease or alter anatomical visibility of the vertebral surface on CT images. Specifically, two types or error may occur during patient alignment: 1) the image registration fails because of a too poor image quality; and 2) the image registration succeeds but the patient alignment fails. The former case can be due to a pathology or metal artifacts altering the CT images and can be assessed by visual inspections after the registration is completed. In the later case, the CT image is no longer representative of the actual anatomy, due to image distortion or partial volume artifacts. Therefore, a good image alignment does not necessarily induces a good patient alignment. While patient misalignment is more difficult to assess visually, CT artifacts can be corrected preoperatively using specific acquisition protocols, physics-based or image-based pre- or post-processing (Barrett and Keat, 2004; Gjesteby et al., 2016). In our study, the quality of the CT images is limited to the clinical standard acquisition protocol with a fixed slice thickness and resolution on a non-pathological animal

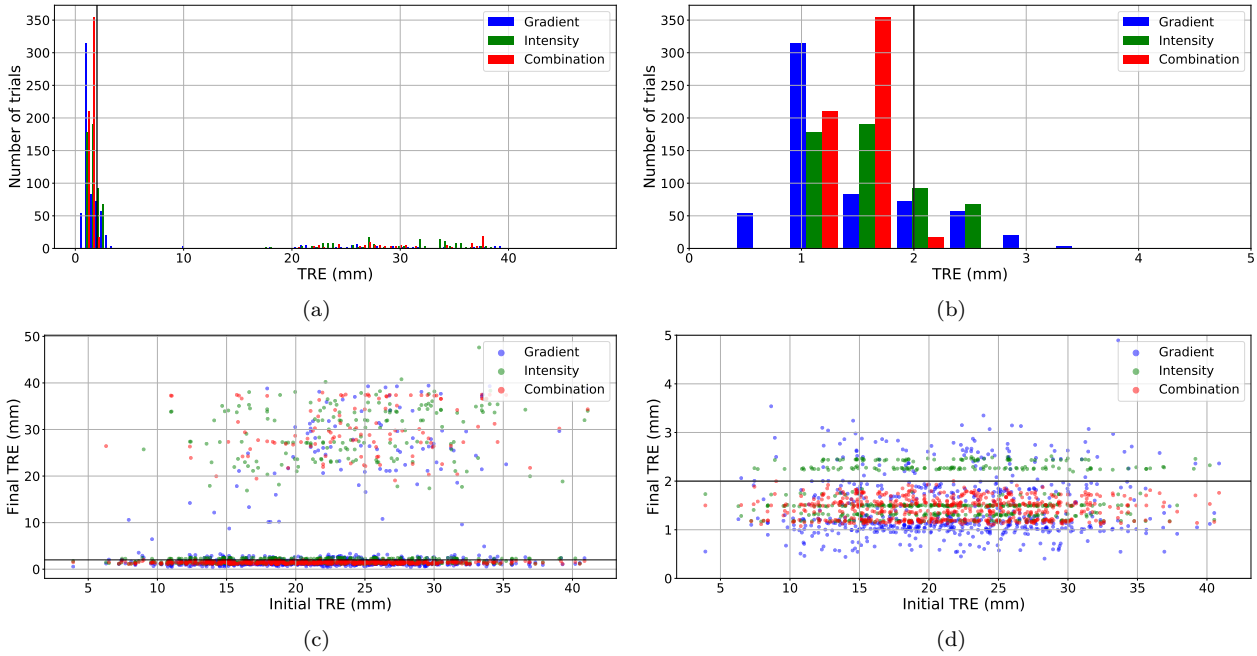

Figure 7: Target registration error distribution: (a) histogram of the TRE, (b) a zoom in of (a) in the range [0 mm, 5 mm], (c) scatter plot of the final TRE according to the initial misalignment TRE, (d) a zoom in of (c) in the range [0 mm, 5 mm]. The 2 mm threshold is indicated by a dark line.

subject, which prevent assessing the effect of such artifacts. Further investigation would be required to understand the limitation of the proposed registration framework in this context.

It is worth noting that the current registration framework does not allow for spine curvature correction as we only consider rigid registration. Group-wise rigid registration of multiple vertebrae has shown promising results on sheep cadavers (Rasoulian et al., 2012; Gill et al., 2012; Nagpal et al., 2015) to compensate for the potential post-operative supine to intra-operative prone spinal curvature. This type of registration requires performing a rigid registration for each single vertebra before adjusting the final registration to account for the global curvature. The fast convergence using the proposed GPU implementation is a good candidate for such an application and will be considered for future work. For now, a practical approach would be to perform a single rigid registration per treated vertebra. Considering a typical 20–30 s to complete the iUS acquisition (Winter et al., 2009), the whole registration procedure can be achieved under 1 minute per vertebral level, minimizing the surgical workflow interruption.

Conclusion

In this paper, we presented an open-source software for iUS guidance in fusion surgery. The platform involves two major components: i) registration of the patient position to the operative field; and ii) visualization of the predicted screw trajectory for vertebra instrumentation. To recover from the loss of navigation accuracy during spinal surgery, the registration procedure needs to be accurate and computationally efficient, so that the surgical workflow does not suffer from frequent interruptions. We have shown that combining gradient orientation and iUS intensity with an initialization based on probe position results in 100 % registration success (i.e., final TRE = 1.47 mm, smaller than the 2 mm clinical threshold) in under 8 seconds on 7 vertebrae of a porcine cadaver. The method is robust and results in 89.86 % and 88.57 % success when partial vertebra is visible on iUS; and 83.14 % success when experimented with initial misalignments of up to

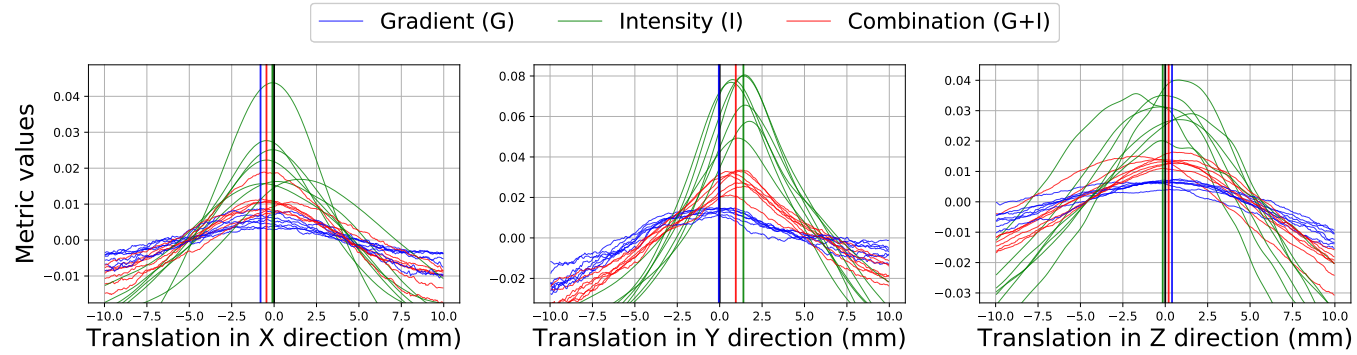

(a)

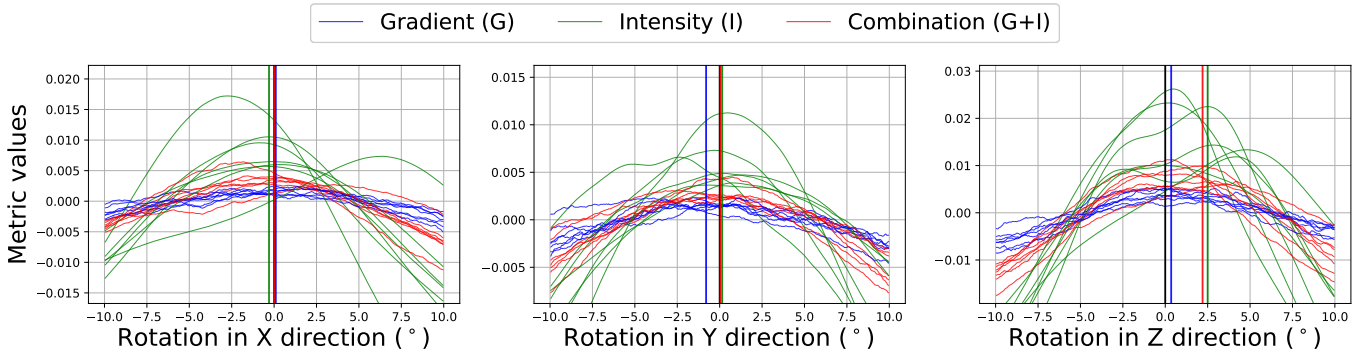

(b)

Figure 8: Results of metric values according to the image misalignments: (a) translationnal misalignment and (b) rotational misalignment.

20 mm and 20°. We believe that the platform will encourage collaborative work and help the development of future iUS-based techniques for guidance in spine interventions. Future work will involve investigating the performance of the multi-metric approach in a slice-to-volume registration framework. This will obviate the need for iUS volume reconstruction, further reducing the intra-operative workload processing.

Supplementary materials

Video 1: Demo video showing the registration and navigation procedures on a spine phantom.
`https://hgueziri.github.io/assets/videos/spineVideo.mp4`

Acknowledgments

This study was funded by grants from the Canadian Institutes of Health Research (246067) and from the Natural Sciences and Engineering Research Council of Canada (396395).

References

Austin MS, Vaccaro AR, Brislin B, Nachwalter R, Hilibrand AS, Albert TJ. Image-Guided Spine Surgery A Cadaver Study Comparing Conventional Open Laminoforaminotomy and Two Image-Guided Techniques for Pedicle Screw Placement in Posterolateral Fusion and Nonfusion Models. Spine, 2002;27:2503–2508.

Barrett JF, Keat N. Artifacts in ct: Recognition and avoidance. RadioGraphics, 2004;24:1679–1691.

Bates D. Fitting linear mixed models in r. R news, 2005;5:27–30.

Besl PJ, McKay ND. A method for registration of 3-d shapes. IEEE Transactions on Pattern Analysis and Machine Intelligence, 1992;14:239–256.

Brendel B, Rick SWA, Stockheim M, Ermert H. Registration of 3d ct and ultrasound datasets of the spine using bone structures. Computer Aided Surgery, 2002;7:146–155.

Brudfors M, Seitel A, Rasoulian A, Lasso A, Lessoway VA, Osborn J, Maki A, Rohling RN, Abolmaesumi P. Towards real-time, tracker-less 3D ultrasound guidance for

spine anaesthesia. International Journal of Computer Assisted Radiology and Surgery, 2015;10:855–865.

Chambers JM, Hastie TJ. Statistical models in S. Wadsworth & Brooks, 1992.

Chan A, Coutts B, Parent E, Lou E. Development and Evaluation of CT-to-3D Ultrasound Image Registration Algorithm in Vertebral Phantoms for Spine Surgery. Annals of Biomedical Engineering, 2020:1–12.

Chen F, Wu D, Liao H. Registration of ct and ultrasound images of the spine with neural network and orientation code mutual information. In: Zheng G, Liao H, Jannin P, Cattin P, Lee SL (Eds.), Medical Imaging and Augmented Reality. Cham, 2016. pp. 292–301.

Cleary K, Anderson J, Brazaitis M, Devey G, DiGioia A, Freedman M, Grönemeyer D, Lathan C, Lemke H, Long D, Mun SK, Taylor R. Final report of the technical requirements for image-guided spine procedures workshop. Computer Aided Surgery, 2000;5:180–215.

Dath R, Ebinesan A, Porter K, Miles A. Anatomical measurements of porcine lumbar vertebrae. Clinical biomechanics (Bristol, Avon), 2007;22:607—613.

De Nigris D, Collins DL, Arbel T. Multi-modal image registration based on gradient orientations of minimal uncertainty. IEEE Transactions on Medical Imaging, 2012;31:2343–2354.

De Nigris D, Collins DL, Arbel T. Fast rigid registration of pre-operative magnetic resonance images to intra-operative ultrasound for neurosurgery based on high confidence gradient orientations. International Journal of Computer Assisted Radiology and Surgery, 2013;8:649–661.

Deyo RA, Nachemson A, Mirza SK. Spinal-fusion surgery—the case for restraint. The Spine Journal, 2004;4:S138 – S142.

Drouin S, Kochanowska A, Kersten-Oertel M, Gerard IJ, Zelmann R, De Nigris D, Bériault S, Arbel T, Sirhan D, Sadikot AF, Hall JA, Sinclair DS, Petrecca K, DelMaestro RF, Collins DL. IBIS: an OR ready open-source platform for image-guided neurosurgery. International Journal of Computer Assisted Radiology and Surgery, 2017;12:363–378.

Fedorov A, Beichel R, Kalpathy-Cramer J, Finet J, Fillion-Robin JC, Pujol S, Bauer C, Jennings D, Fennessy F, Sonka M, Buatti J, Aylward S, Miller JV, Pieper S, Kikinis R. 3d slicer as an image computing platform for the quantitative imaging network. Magnetic resonance imaging, 2012;30:1323–1341.

Gebhard F, Weidner A, Liener UC, Stöckle U, Arand M. Navigation at the spine. Injury, 2004;35:35 – 45.

Gill S, Abolmaesumi P, Fichtinger G, Boisvert J, Pichora D, Borshneck D, Mousavi P. Biomechanically constrained groupwise ultrasound to CT registration of the lumbar spine. Medical Image Analysis, 2012;16:662–674.

Gjesteby L, De Man B, Jin Y, Paganetti H, Verburg J, Giantsoudi D, Wang G. Metal artifact reduction in ct: Where are we after four decades? IEEE Access, 2016;4:5826–5849.

Gueziri HE, Collins DL. Fast registration of ct with intraoperative ultrasound images for spine surgery. In: Computational Methods and Clinical Applications for Spine Imaging. Springer International Publishing, 2019. pp. 29–40.

Gueziri HE, Drouin S, Yan CXB, Collins DL. Toward real-time rigid registration of intra-operative ultrasound with preoperative ct images for lumbar spinal fusion surgery. International Journal of Computer Assisted Radiology and Surgery, 2019.

Gueziri HE, Santaguida C, Collins DL. Thestate-of-the-art in ultrasound-guided spine interventions. Medical Image Analysis, 2020;65:101769.

Hacihaliloglu I. Ultrasound imaging and segmentation of bone surfaces: A review. Technology, 2017;05:74–80.

Hansen N, Ostermeier A. Completely derandomized self-adaptation in evolution strategies. Evolutionary computation, 2001;9:159–195.

Jain AK, Taylor RH. Understanding bone responses in B-mode ultrasound images and automatic bone surface extraction using a Bayesian probabilistic framework. In: Walker WF, Emelianov SY (Eds.), Medical Imaging 2004: Ultrasonic Imaging and Signal Processing. Vol. 5373. International Society for Optics and Photonics, SPIE, 2004. pp. 131 – 142.

Ji S, Fan X, Paulsen KD, Roberts DW, Mirza SK, Lollis SS. Patient registration using intraoperative stereovision in image-guided open spinal surgery. IEEE Transactions on Biomedical Engineering, 2015;62:2177–2186.

Khallaghi S, Mousavi P, Gong RH, Gill S, Boisvert J, Fichtinger G, Pichora D, Borschneck D, Abolmaesumi P. Registration of a statistical shape model of the lumbar spine to 3d ultrasound images. In: Medical Image Computing and Computer-Assisted Intervention – MICCAI 2010. Springer Berlin Heidelberg, 2010. pp. 68–75.

Klein S, Staring M, Murphy K, Viergever MA, Pluim JPW. elastix: A toolbox for intensity-based medical image registration. IEEE Transactions on Medical Imaging, 2010;29:196–205.

Koo TK, Kwok WE. Hierarchical CT to Ultrasound Registration of the Lumbar Spine: A Comparison with Other Registration Methods. Annals of Biomedical Engineering, 2016;44:2887–2900.

Lang A, Mousavi P, Gill S, Fichtinger G, Abolmaesumi P. Multi-modal registration of speckle-tracked freehand 3D ultrasound to CT in the lumbar spine. Medical Image Analysis, 2012;16:675–686.

Lasso A, Heffter T, Rankin A, Pinter C, Ungi T, Fichtinger G. Plus: Open-source toolkit for ultrasound-guided intervention systems. IEEE Transactions on Biomedical Engineering, 2014;61:2527–2537.

McCullagh P, Nelder J. Generalized linear models. Chapman and Hill, 1989.

Mercier L, Del Maestro RF, Petrecca K, Kochanowska A, Drouin S, Yan CX, Janke AL, Chen SJS, Collins DL. New prototype neuronavigation system based on preoperative imaging and intraoperative freehand ultrasound: system description and validation. International journal of computer assisted radiology and surgery, 2011;6:507–522.

Moghari MH, Abolmaesumi P. Point-based rigid-body registration using an unscented kalman filter. IEEE Transactions on Medical Imaging, 2007;26:1708–1728.

Muratore DM, Russ JH, Dawant BM, Galloway RL. Three-dimensional image registration of phantom vertebrae for image-guided surgery: A preliminary study. Computer Aided Surgery, 2002;7:342–352.

Myronenko A, Song X. Point set registration: Coherent point drift. IEEE Transactions on Pattern Analysis and Machine Intelligence, 2010;32:2262–2275.

Nagpal S, Abolmaesumi P, Rasoulian A, Hacihaliloglu I, Ungi T, Osborn J, Lessoway VA, Rudan J, Jaeger M, Rohling RN, Borschneck DP, Mousavi P. A multivertebrae ct to us registration of the lumbar spine in clinical data. International Journal of Computer Assisted Radiology and Surgery, 2015;10:1371–1381.

Quené H, van den Bergh H. Examples of mixed-effects modeling with crossed random effects and with binomial data. Journal of Memory and Language, 2008;59:413 – 425.

Quiñones-Hinojosa A, Kolen ER, Jun P, Rosenberg WS, Weinstein PR. Accuracy over space and time of computer-assisted fluoroscopic navigation in the lumbar spine in vivo. Clinical Spine Surgery, 2006;19:109–113.

Rasoulian A, Abolmaesumi P, Mousavi P. Feature-based multibody rigid registration of CT and ultrasound images of lumbar spine. Medical Physics, 2012;39:3154–3166.

Rasoulian A, Seitel A, Osborn J, Sojoudi S, Nouranian S, Lessoway VA, Rohling RN, Abolmaesumi P. Ultrasound-guided spinal injections: a feasibility study of a guidance system. International Journal of Computer Assisted Radiology and Surgery, 2015;10:1417–1425.

Roche A, Pennec X, Malandain G, Ayache N. Rigid registration of 3-d ultrasound with mr images: a new approach combining intensity and gradient information. IEEE Transactions on Medical Imaging, 2001;20:1038–1049.

Sheng SR, Wang XY, Xu HZ, Zhu GQ, Zhou YF. Anatomy of large animal spines and its comparison to the human spine: a systematic review. European Spine Journal, 2010;19:46–56.

Smith ZA, Sugimoto K, Lawton CD, Fessler RG. Incidence of Lumbar Spine Pedicle Breach After Percutaneous Screw Fixation A Radiographic Evaluation of 601 Screws in 151 Patients. Journal of Spinal Disorders and Techniques, 2014;27:358–363.

Stieglitz LH, Fichtner J, Andres R, Schucht P, Krähenbühl AK, Raabe A, Beck J. The Silent Loss of Neuronavigation Accuracy: A Systematic Retrospective Analysis of Factors Influencing the Mismatch of Frameless Stereotactic Systems in Cranial Neurosurgery. Neurosurgery, 2013;72:796–807.

Stone JE, Gohara D, Shi G. Opencl: A parallel programming standard for heterogeneous computing systems. Computing in Science Engineering, 2010;12:66–73.

Takahashi S, MoriKawa S, Saruhashi Y, MatsUsue Y, Kawakami M. Percutaneous transthoracic fenestration of an intramedullary neurenteric cyst in the thoracic spine with intraoperative magnetic resonance image navigation and thoracoscopy. Journal of Neurosurgery: Spine, 2008;9:488–492.

Takahashi S, Saruhashi Y, Odate S, Matsusue Y, Morikawa S. Percutaneous aspiration of spinal terminal ventricle cysts using real-time magnetic resonance imaging and navigation. Spine, 2009;34:629–634.

Tatsui CE, Nascimento CNG, Suki D, Amini B, Li J, Ghia AJ, Thomas JG, Stafford RJ, Rhines LD, Cata JP, Kumar AJ, Rao G. Image guidance based on mri for spinal interstitial laser thermotherapy: technical aspects and accuracy. Journal of Neurosurgery: Spine, 2017;26:605–612.

Tokuda J, Fischer GS, Papademetris X, Yaniv Z, Ibanez L, Cheng P, Liu H, Blevins J, Arata J, Golby AJ, et al. Openigtlink: an open network protocol for image-guided therapy environment. The International Journal of Medical Robotics and Computer Assisted Surgery, 2009;5:423–434.

Ungi T, Abolmaesumi P, Jalal R, Welch M, Ayukawa I, Nagpal S, Lasso A, Jaeger M, Borschneck DP, Fichtinger G, Mousavi P. Spinal needle navigation by tracked ultrasound snapshots. IEEE Transactions on Biomedical Engineering, 2012;59:2766–2772.

Ungi T, Moult E, Schwab JH, Fichtinger G. Tracked ultrasound snapshots in percutaneous pedicle screw placement navigation: A feasibility study. Clinical Orthopaedics and Related Research, 2013;471:4047–4055.

Wein W, Brunke S, Khamene A, Callstrom MR, Navab N. Automatic CT-ultrasound registration for diagnostic imaging and image-guided intervention. Medical Image Analysis, 2008;12:577–585.

Wein W, Karamalis A, Baumgartner A, Navab N. Automatic bone detection and soft tissue aware ultrasound-CT registration for computer-aided orthopedic surgery. International Journal of Computer Assisted Radiology and Surgery, 2015;10:971–979.

Winter S, Brendel B, Pechlivanis I, Schmieder K, Igel C. Registration of ct and intraoperative 3-d ultrasound images of the spine using evolutionary and gradient-based methods. IEEE Transactions on Evolutionary Computation, 2008;12:284–296.

Winter S, Pechlivanis I, Dekomien C, Igel C, Schmieder K. Toward registration of 3D ultrasound and CT images of the spine in clinical praxis: design and evaluation of

a data acquisition protocol. Ultrasound in medicine & biology, 2009;35:1773–1782.

Woodard EJ, Leon SP, Moriarty TM, Quinones A, Zamani AA, Jolesz FA. Initial experience with intraoperative magnetic resonance imaging in spine surgery. Spine, 2001;26:410–417.

Yan CX, Goulet B, Pelletier J, Chen SJS, Tampieri D, Collins DL. Towards accurate, robust and practical ultrasound-CT registration of vertebrae for image-guided spine surgery. International Journal of Computer Assisted Radiology and Surgery, 2011;6:523–537.

Yan CX, Goulet B, Tampieri D, Collins DL. Ultrasound-CT registration of vertebrae without reconstruction. International Journal of Computer Assisted Radiology and Surgery, 2012a;7:901–909.

Yan CXB, Goulet B, Chen SJS, Tampieri D, Collins DL. Validation of automated ultrasound-CT registration of vertebrae. International Journal of Computer Assisted Radiology and Surgery, 2012b;7:601–610.

Yoo TS, Ackerman MJ, Lorensen WE, Schroeder W, Chalana V, Aylward S, Metaxas D, Whitaker R. Engineering and algorithm design for an image processing api: a technical report on itk-the insight toolkit. Studies in health technology and informatics, 2002:586–592.